Integrated Structural and Nature-Based Defense Systems to Reduce Tsunami Inundation under a Megathrust Scenario

Yudhi Prabowo

yudhi.prabowo86@gmail.com

National Research and Innovation Agency Republic of Indonesia (BRIN) https://orcid.org/0009-0003-6502-0088

Widjo Kongko

National Research and Innovation Agency Republic of Indonesia (BRIN)

Mardi Wibowo

National Research and Innovation Agency Republic of Indonesia (BRIN)

Imam Fachrudin

National Research and Innovation Agency Republic of Indonesia (BRIN)

Fajar Yulianto

National Research and Innovation Agency Republic of Indonesia (BRIN)

Edwin Adi Wiguna

National Research and Innovation Agency Republic of Indonesia (BRIN)

Hanah Khoirunnisa

National Research and Innovation Agency Republic of Indonesia (BRIN)

Marindah Yulia Iswari

National Research and Innovation Agency Republic of Indonesia (BRIN)

Hilmi Aziz

National Research and Innovation Agency Republic of Indonesia (BRIN)

Nurkhalis Rahili

National Research and Innovation Agency Republic of Indonesia (BRIN)

Research Article

Keywords: tsunami inundation, numerical modelling, tsunami mitigation scenario, megathrust, seawall, nature-based solution

Posted Date: November 13th, 2025

DOI: https://doi.org/10.21203/rs.3.rs-7637400/v1

Version of Record: A version of this preprint was published at Natural Hazards on April 27th, 2026. See the published version at https://doi.org/10.1007/s11069-026-08148-z.

Title:

Integrated Structural and Nature-Based Defense Systems to Reduce Tsunami Inundation under a Megathrust Scenario

Authors:

Yudhi Prabowo[1*], Widjo Kongko[1], Mardi Wibowo[1], Imam Fachrudin[1], Fajar Yulianto[1,2], Edwin A. Wiguna[1,3], Hanah Khoirunnisa [1,4], Marindah Y. Iswari[1], Hilmi Aziz[1,3], Nurkhalis Rahili[1,3]

Affiliations:

[1]Research Center for Hydrodynamics Technology, National Research and Innovation Agency (BRIN), Serpong, Indonesia

[2]Doctoral Program in Geography, Faculty of Geography, Universitas Gadjah Mada, Yogyakarta, Indonesia

[3]Department of Geodetic Engineering, Faculty of Engineering, Universitas Gadjah Mada, Yogyakarta, Indonesia

[4]Department of Civil Engineering, Faculty of Civil and Environmental Engineering, Institut Teknologi Bandung, Bandung, Indonesia

***Corresponding author:**

Yudhi Prabowo (yudhi.prabowo@brin.go.id)

Abstract

Coastal regions located near subduction zones are highly exposed to megathrust-generated tsunamis that threaten coastal communities and critical infrastructures. This study investigates the effectiveness of structural, nature-based, and hybrid defense systems in mitigating tsunami inundation under a worst-case scenario of a Mw 8.8 subduction earthquake. Using available high-resolution bathymetric and topographic data, eight mitigation scenarios were simulated, including seawalls of 5, 10, and 15 meters in height and a 200-meter-wide Casuarina equisetifolia forest belt, individually and in combination. Results indicate that vegetation alone and low seawalls offer limited protection, while a 10-meter seawall substantially reduces inundation area and depth. The 15-meter seawall provides the highest level of protection, almost eliminating tsunami flooding across critical facilities. When combined with vegetation, the hybrid approach enhances performance by dissipating overtopping energy and reducing residual flooding. Temporal analyses reveal that higher seawalls also delay tsunami arrival, providing valuable time for emergency response. These findings highlight the importance of multi-layered, hybrid mitigation strategies that integrate engineered structures with ecological components to enhance the resilience of coastal infrastructure. The study provides insights that can inform global efforts to protect vital coastal assets from future megathrust tsunami events.

Keywords:

tsunami inundation, numerical modelling, tsunami mitigation scenario, megathrust, seawall, nature-based solution

1. Introduction

Tsunamis are a great threat to the coastal areas affecting by seismic zones. Although the probability of seismic tsunami occurrence is low, once it occurs, it may cause catastrophic damage and heavy casualties. Over the past two decades, Indonesia has endured several major tsunami disasters that have left deep scars on the nation's history. The 26 December 2004 Indian Ocean tsunami, triggered by a massive Mw 9.3 megathrust earthquake off the coast of Sumatra (Rabinovich et al. 2006; Lauterjung et al. 2010), remains one of the deadliest natural disasters in recorded history. The waves propagated across the Indian Ocean, claiming more than 230,000 lives in multiple countries (Bernard and Titov 2015), with Indonesia suffering the largest number of fatalities. In addition to the staggering human toll, the event caused unprecedented economic losses, displaced millions of people, and severely damaged coastal ecosystems.

Other tsunami events in Indonesia have demonstrated the diversity of tsunami generation mechanisms. For example, the 2018 Palu tsunami was primarily triggered by an underwater landslide associated with a strike-slip earthquake (Setyonegoro et al. 2024; Heidarzadeh and Mulia 2022), whereas the December 2018 Sunda Strait tsunami resulted from a slope collapse of the Anak Krakatau volcano (Dogan et al. 2021; Muhari et al. 2019). Both events occurred without significant ground shaking in some affected areas, which reduced the effectiveness of conventional earthquake-based early warning systems. These tsunamis caused hundreds of deaths, thousands of injuries, and the destruction of critical infrastructure. This further illustrates the urgent need for comprehensive mitigation strategies tailored to Indonesia's unique hazard profile.

One region of particular concern is the southern part of Java Island, which is directly influenced by the tectonic dynamics of the Sunda Subduction Zone (Luschen et al. 2011; Xie et al. 2023). In this zone, the Indo-Australian Plate subducts beneath the Eurasian Plate, potentially creating an extensive megathrust fault capable of generating massive earthquakes and tsunamis. The Central Java–East Java segment of the subduction zone has experienced several large-magnitude seismic events in the past century, including the Mw 8.1 earthquake in 1916 (Griffin et al. 2019), the Mw

7.8 earthquake in 1994 (Synolakis et al. 1995), and the Mw 7.7 earthquake in 2006 (Lavigne et al. 2007). Historical and geological evidence suggest that the recurrence of such events is inevitable. Seismologists have warned that a future Mw 8.8 earthquake could occur along this segment, producing a tsunami with devastating impacts (Irsyam et al. 2017; Widiyantoro et al. 2020; Zhao et al. 2025; Harris et al. 2024).

Yogyakarta International Airport (YIA) is a critical infrastructure located within this high risk coastal zone (Kongko and Hidayat 2014). Situated on the southern coast of Central Java, YIA lies within the modeled tsunami inundation area for potential large magnitude offshore earthquakes. The airport was constructed as a replacement for Adisutjipto International Airport to accommodate higher passenger volumes, larger aircraft, and international routes, thereby supporting the region's economic growth and tourism sector. Beyond its economic role, YIA has strategic importance for disaster management, serving as a hub for evacuation operations, logistical support for humanitarian aid deployment, and the distribution of emergency supplies during crises (Dewatama and Ikaputra 2021). However, its proximity to the coastline and its location within a tsunami hazard zone make it highly vulnerable to wave impacts and structural damage. Numerical simulations and hazard assessments indicated that tsunami wave heights in this region could reach up to 20 meters in the worst case scenario (Prabowo et al. 2024; Wulandani et al. 2024), posing a severe threat to airport facilities and surrounding communities.

Given these risks, the protection of YIA and its surrounding area requires a combination of engineered defenses and nature-based solutions. Structural measures such as seawalls have been employed in tsunami-prone countries, such as Japan (Raby et al. 2015) and Netherlands (de Ruig 1998), to provide immediate physical barriers against incoming waves. Properly designed and constructed seawalls may reduce inundation depth and velocity, thereby minimizing damage to infrastructure located behind them. However, seawalls alone may not be sufficient, as they can be overtopped or structurally compromised during extreme events. Additionally, their construction and maintenance require substantial financial investment and may have ecological consequences.

In recent years, there has been increasing recognition of the importance of integrating nature-based solutions into coastal defense systems (Zanin et al. 2024; Boulenger et al. 2024). Coastal vegetation, particularly dense tree belts, may provide sustainable and multifunctional protection against ocean waves while also offering ecological and social benefits (van Veelen et al. 2021; Haghdoost and Azamathulla 2024). Among the various species considered for such purposes, *Casuarina equisetifolia* (commonly known as "Cemara udang" tree in Indonesia) has shown considerable potential in attenuating wave energy (Samarakoon et al. 2013; Chen et al. 2025). This tree species thrives in sandy and saline environments, exhibits high wind resistance, and contributes to coastal soil stabilization through its extensive root systems. Previous studies have demonstrated that *Casuarina* belts may reduce the strength and depth of wave inundation, particularly when planted in wide and dense configurations (Samarakoon et al. 2013; Tanaka et al. 2007). The effectiveness of such vegetation barriers depends on several factors, including tree height, trunk diameter, spacing, density, and the width of the belt (Chen et al. 2025; Mukherjee et al. 2023). Moreover, *Casuarina* trees can be integrated with other protective features, such as sand dunes (Ndiaye et al. 1993; Martínez and Kolega 2013) or engineered structures (Morris et al. 2023; Lawrence and Nandasena 2019), to form hybrid defense systems that enhance resilience while preserving coastal landscapes.

The novelty of this study lies in the multi-mitigation scenario modeling using the highest available spatial-resolution bathymetric and topographic data applied to the Yogyakarta International Airport area, one of Indonesia's most strategic coastal infrastructures. This study aims to assess the effectiveness of various mitigation scenarios involving a *Casuarina* tree belt and seawall, both individually and in combination. Using numerical modeling techniques, we simulated tsunami inundation patterns under different mitigation scenarios to assess their capacity in reducing hazard exposure. The analysis considers several performance indicators, including the maximum inundation depth, spatial extent of flooding, arrival time of tsunami waves, and the reduction in inundation area relative to the unprotected baseline scenario. By addressing the performance of hybrid defenses in the context of a modern airport, this work contributes to the global body of knowledge on tsunami risk reduction for critical coastal infrastructure.

2. Materials and methods

2.1. Site description

The research study focuses on the coastal areas around Yogyakarta International Airport (YIA), Indonesia. YIA is a major transportation hub that began operating in 2019, replacing Adisutjipto International Airport as the main airport. Geographically, the airport area is very close to the coastline with a distance of about 900 meters from the coastline and is flanked by two rivers on its east and west sides: the Bogowonto River (west) and the Serang River (east). When a tsunami occurs, the presence of these two major rivers may pose a significant risk as they can influence the direction, extent, and distribution of tsunami wave propagation around the airport area.

This study was conducted along a 14-kilometers stretch of coastline (see **Fig. 1**). The coastline is characterized by a straight shoreline, primarily oriented toward the south–southwest. There is a slight difference in the bathymetric profile between the western and eastern sides of the airport. On the western side, the seafloor drops off sharply offshore, whereas on the eastern side it slopes more gradually. The topographic is generally flat, with terrain elevations ranging from 0 to 36 meters above mean sea level and an average elevation of approximately 8 meters.

The land cover across the sand dunes is predominantly composed of agricultural land and forested areas, with *Casuarina equisetifolia* being the dominant tree species of the forest.

Fig. 1. Study area

Fig. 1 illustrates the research location used to determine the proximity of the subduction zone to Yogyakarta International Airport. The airport area lies within the subduction zone, which is formed by the convergence of the two tectonic plates. When a major offshore earthquake occurs, it can generate tsunami waves that can reach the coast within minutes, leaving little time for evacuation or emergency response. The speed of tsunami wave propagation is influenced by ocean depth. In deep waters, waves can travel faster and reach hundreds to thousands of kilometers per hour with low wave heights. In contrast, as the waves approach shallow coastal areas, their speed decreases and wave heights increase (Tandel et al. 2022; Varsoliwala and Singh 2021; Kakinuma and Kosugi 2025).

2.2. Tsunami simulations

This study employed the Non-Linear Shallow Water Equations (NLSWE) using the TUNAMI-N3 model. TUNAMI-N3 is a modified version of TUNAMI-N2 (Imamura et al. 1995), which is based on linear theory in deep ocean, shallow water theory in coastal regions, and runup processes on land using variable grid resolutions (Heidarzadeh et al. 2009; Harig et al. 2008). TUNAMI does not directly use fault data, but requires an initial wave derived from a fault model.

The tsunami scenario modeled in this study was generated using a hypothetical megathrust earthquake with a magnitude of Mw 8.8 (Irsyam et al. 2017), located along the southern Java subduction zone. This event was designed to reflect the worst case scenario based on historical seismicity for this study area. The earthquake source was modeled using a multi-segment fault approach which consists of three fault segments. Each segment was defined by specific geophysical parameters, including location, depth, fault geometry, and rigidity. The earthquake fault parameters are presented in **Table 1**. Vertical seafloor displacements (D) resulting from this fault configuration were calculated using the Okada (1985) model. The fault dimension (L and W) was determined using the method of Wells and Coppersmith (1994) empirical relations, while rigidity values were set as depth-dependent and calculated following the approach of Lay et al. (2012) The resulting seafloor uplift and subsidence were then used as initial conditions for tsunami generation in the numerical model (**Fig. 2**). This fault configuration was used to represent a large-scale faulting event that could generate tsunami waves with the potential for significant inundation on land.

Table 1
The fault parameters of the seismic event used for the tsunami simulation

Scenario Mag [Mw]	Fault	Epicenter		Mag [Mw]	Depth [Km]	Strike [Deg]	Dip [Deg]	Slip [Deg]	L [Km]	W [Km]	D [Km]	Rigidity [Gpa]
		Longitude	Latitude									
8.8	1	108.320291	-9.096980	8.5	23.0	288.0	10.0	90.0	160.0	100.0	18.0	26
	2	109.797659	-9.457861	8.6	22.0	279.0	16.0	90.0	160.0	100.0	22.5	24
	3	111.333233	-9.552373	8.5	23.0	268.0	16.0	90.0	160.0	100.0	18.0	26

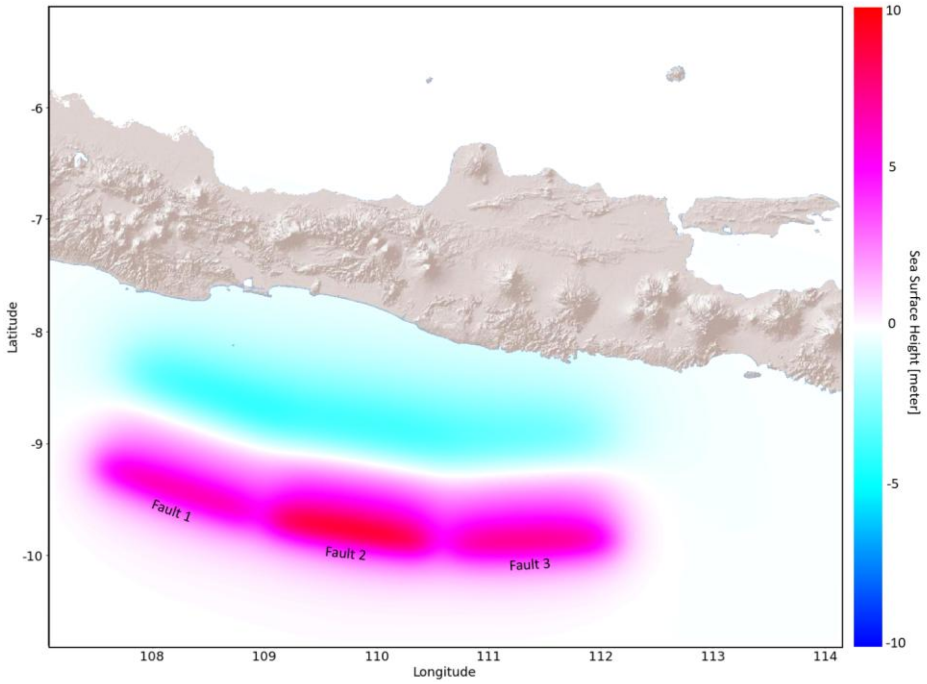

Fig 2. Initial tsunami wave height at the source of the earthquake

A multi-domain (nested grid) system was implemented to simulate the tsunami wave propagation from its source to the area of interest with increasing spatial detail (**Fig. 3**). The system consists of five computational domains with progressively finer spatial resolutions at each domain level (**Table 2**). The resolution ratio between successive domains was set at 3:1. Domain 1 has the coarsest resolution and was designed to cover the initial tsunami wave propagation in the deep ocean, while Domain 5 has the finest. The coarsest domain (Domain 1) has a spatial resolution of 21.016 arc seconds (approximately 648 meters) and encompasses a wide area from 5.19°S to 10.90°S and 107.06°E to 114.13°E. As the waves propagate toward the coast, the simulation transitions through increasingly finer domains: Domain 2, Domain 3, Domain 4, and Domain 5. The finest domain (Domain 5) has a resolution of 0.259 arc seconds (approximately 8 meters) and was used to simulate detailed inundation dynamics in the YIA area. In all domains, both water depth and land elevation are referenced to mean sea level, which is also assumed to represent the ambient sea level for the tsunami simulation.

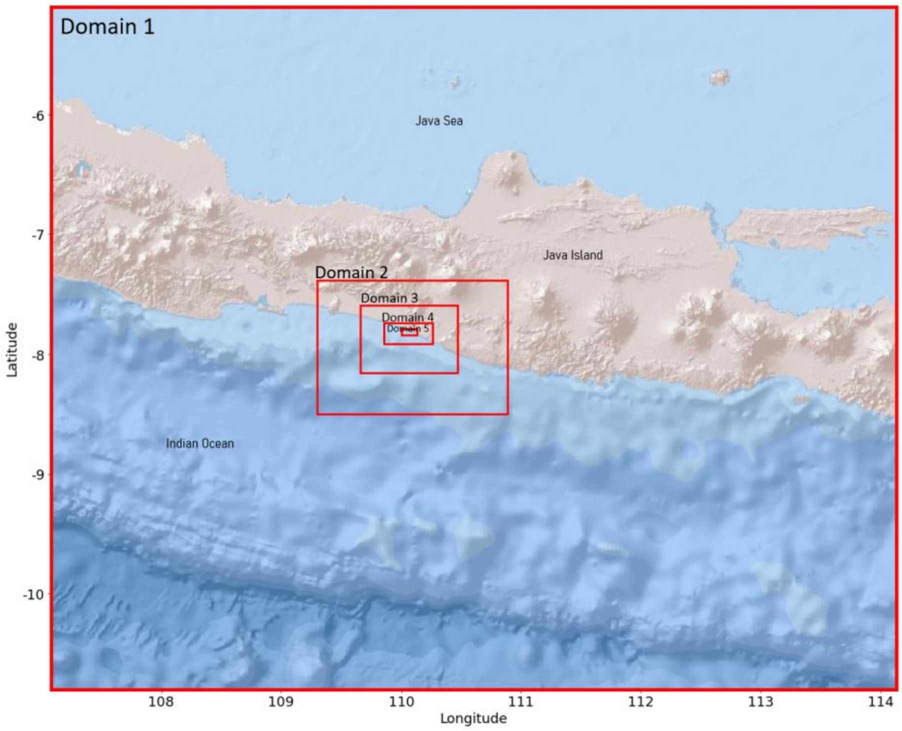

Fig. 3. Configuration of the nested grid system used in the numerical simulation. The model consists of five computational domains (Domain 1 to Domain 5), each with increasingly finer spatial resolution, centered around the southern coast of Java Island near Yogyakarta International Airport.

Table 2

Detailed parameters of the nested grid system used in the tsunami simulations

Domain	Domain coverage		Domain resolution (dx, dy)		Time step (dt)	Tsunami model
	Top left	Bottom right	[arc second]	[meter]	[second]	
1	107.0679, -5.1982	114.1376, -10.9018	21.016	648	1.0	Linear
2	109.3032, -7.4899	110.8541, -8.58550	7.005	216	0.8	Linear
3	109.6649, -7.6863	110.4687, -8.24420	2.335	72	0.5	Linear
4	109.8530, -7.8227	110.2484, -8.01000	0.778	24	0.3	Non linear
5	109.9988, -7.8771	110.1142, -7.93620	0.259	8	0.2	Non linear

In this study, we conducted a series of tsunami mitigation simulations using seawalls of varying heights and coastal vegetation, specifically *Casuarina equisetifolia*. All tsunami simulations were carried out over a 90-minute period to model wave propagation from the offshore earthquake source to the study area. These scenarios aim to evaluate the effectiveness of structural and nature-based solutions in reducing tsunami inundation, either individually or in combination. The series of tsunami mitigation simulations conducted in this study are as follows:

1. Baseline Scenario (No Barriers)
   This scenario represents the existing natural conditions without any structural or vegetative barriers. Surface roughness was defined solely based on existing land cover classifications. This baseline scenario serves as a reference for assessing the effectiveness of the following seven mitigation scenarios.
2. *Casuarina* Forest
   This scenario adopts a nature-based solution by modeling a 200-meter-wide dense forest barrier of *Casuarina equisetifolia* trees along the coastline as a natural defense mechanism. The vegetation is characterized by specific physical attributes, such as trunk diameter, tree density, and height, which increase surface roughness and friction. This roughness is expected to slow down and dissipate the energy of incoming tsunami waves, thereby reducing both the extent and depth of inundation on land.
3. 5-Meter High Seawall
4. 10-Meter High Seawall
5. 15-Meter High Seawall
   Three seawalls of varying heights were implemented to block tsunami wave propagation and reduce inland inundation. Seawalls are modeled as a rigid, impermeable structure aligned along the coastline. These scenarios investigate whether increasing wall height would continue to yield significant reductions in tsunami impact.
6. Combination of *Casuarina* Forest and 5-Meter High Seawall
7. Combination of *Casuarina* Forest and 10-Meter High Seawall
8. Combination of *Casuarina* Forest and 15-Meter High Seawall
   These three scenarios simulate hybrid mitigation systems by combining the vegetation barrier with the seawalls of varying heights to simulate the maximum protection that may be achieved through an integrated approach. It is used to assess the effectiveness of combining natural and structural defenses in extreme scenarios.

In the numerical simulation, the effect of the coastal forest is represented as a resistance force, composed of both drag and inertia components. Equations (1) and (2) are the resistance coefficients, where C_D is the drag coefficient; V_o is the volume of tree under water surface in a constant volume; V is the volume of water in a constant volume; C_M is the inertia coefficient.

$$C_D = 8.4\frac{V_0}{V} + 0.66 \quad \left(0.01 \leq \frac{V_0}{V} \leq 0.07\right) \tag{1}$$

$$C_M = 1.7 \tag{2}$$

To examine the tsunami attenuation effect provided by coastal forests, numerical simulations of tsunami run-up were performed, incorporating the resistance effect of the modeled forest. The governing equation used for the numerical simulation is the momentum equation in x and y directions (3) and (4) with the hydraulic resistance force by coastal forest, which is modelled by Morison's equation (Harada and Imamura 2000). where: M and N is the flux discharge; D is the total depth; η is the water level; n is the Manning roughness coefficient; A_0 is the projected area of trees under the water; Δx and Δy is the grid spatial size and g is the gravitational acceleration.

$$\frac{\partial M}{\partial t} + \frac{\partial}{\partial x}\left(\frac{M^2}{D}\right) + \frac{\partial}{\partial y}\left(\frac{MN}{D}\right) + gD\frac{\partial \eta}{\partial x} + \frac{gn^2}{D^{7/3}}M\sqrt{M^2+N^2} + \frac{C_D}{2}\frac{A_0}{\Delta x.\Delta y}\frac{M\sqrt{M^2+N^2}}{D^2} + C_M\frac{V_0}{V}\frac{\partial M}{\partial t} = 0 \tag{3}$$

$$\frac{\partial N}{\partial t} + \frac{\partial}{\partial x}\left(\frac{N^2}{D}\right) + \frac{\partial}{\partial y}\left(\frac{MN}{D}\right) + gD\frac{\partial \eta}{\partial x} + \frac{gn^2}{D^{7/3}}N\sqrt{M^2+N^2} + \frac{C_D}{2}\frac{A_0}{\Delta x.\Delta y}\frac{N\sqrt{M^2+N^2}}{D^2} + C_M\frac{V_0}{V}\frac{\partial N}{\partial t} = 0 \tag{4}$$

2.3. Data preparation

Modeling tsunami inundation is influenced by several factors, including topographic slope (Yamaguchi and Sekiguchi 2015; Fathianpour et al. 2024), earthquake source strength (Cheng and Weiss 2013; Geist and Yoshioka 1996), the distance between the study area and the source (Yoshii et al. 2018; Satake et al. 2022), the surface roughness coefficient (Wuthrich et al. 2019; Kaiser et al. 2011), and the simulation duration (Yoshii et al. 2017; Fukutani et al. 2023). These parameters were used to calculate the extent of inundation on land. This study employed a combination of high-resolution bathymetric and topographic datasets to simulate tsunami wave propagation and inundation. The bathymetric data were obtained from BATNAS with a spatial resolution of 6 arc seconds, while topographic data were sourced from DEMNAS with a finer resolution of 0.27 arc seconds. Both datasets were provided by the Geospatial Information Agency (Badan Informasi Geospasial 2024). To accurately simulate tsunami wave propagation and inundation, the bathymetric and topographic data were integrated into a unified elevation model. Bathymetric data are generally reliable for oceanic regions but less accurate for land elevations. Conversely, topographic data provide accurate representations of terrestrial areas but are inadequate for underwater terrain. In this study, both datasets were merged to generate a comprehensive digital elevation model (DEM) that captures the full terrain profile from deep sea regions to inland areas. Since bathymetric and topographic data typically originate from different sources and have varying spatial resolutions, a resampling procedure was conducted prior to integration. Bilinear interpolation was applied to resample both datasets to a resolution suitable for tsunami modeling. Elevation values for water-covered areas were exclusively derived from the bathymetric dataset, while those for land areas were obtained from the topographic dataset.

To simulate tsunami mitigation scenarios involving seawalls, the DEM needs to be modified to represent the presence of a tall artificial coastal barrier (**Fig. 4**). The seawall, approximately 10 kilometers in length and 20 meters in thickness, is designed to protect infrastructure within the airport area. Specifically, elevation values along the designated seawall were elevated according to the intended seawall heights: 5 meters, 10 meters, and 15 meters above mean sea level. The placement of the seawall was determined based on a buffer zone along the coastline adjacent to vital infrastructure, particularly around the YIA area. To reflect its artificial surface characteristics, the Manning's roughness coefficient for the seawall area was set to 0.06. This value, corresponding to man-made structures such as concrete walls, accounts for the increased surface resistance typically associated with engineered constructions. The integration of modified elevation data and seawall parameters enables the simulation model to realistically represent coastal defense measures. These adjustments are essential for assessing the effectiveness of structural mitigation under various tsunami hazard conditions. By modifying both elevation and surface roughness parameters, the model can more accurately simulate the blocking of water inundation, thereby supporting comprehensive tsunami risk assessments for nearshore infrastructure such as airports.

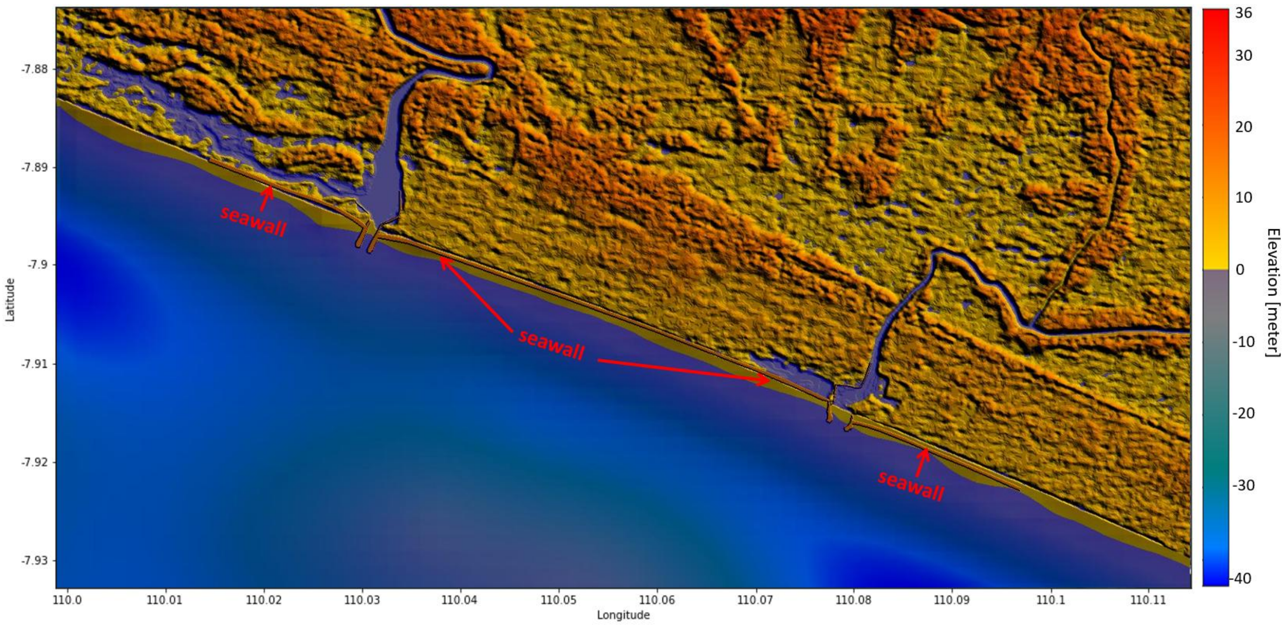

Fig. 4. Modification of the Digital Elevation Model (DEM) to represent the presence of seawall structures along the coastline. The seawalls are indicated with red annotations.

In addition to bathymetric and topographic data, land cover information also plays a critical role in accurately modeling flow resistance during tsunami wave propagation. This resistance is commonly represented by the Manning's roughness coefficient, which influences the velocity and behavior of tsunami waves as they travel across land surfaces (Kaiser et al. 2011; Bricker et al. 2015). Therefore, an accurate representation of surface characteristics is essential for enhancing the reliability of numerical simulations. In this study, surface roughness values were derived from land cover maps that were manually digitized through visual interpretation of high-resolution Google satellite imagery. Various land cover types in the area surrounding Yogyakarta International Airport were identified and classified using Geographic Information System (GIS) software. Land cover under existing conditions was categorized into four distinct classes: water, open flat land, vegetation, and man-made buildings (**Fig. 5**). Each pixel cell was assigned a Manning's roughness coefficient corresponding to its land cover class. The roughness values for water, open flat land, vegetation, and man-made buildings were set to 0.025, 0.036, 0.046, and 0.06, respectively (**Table 3**). Furthermore, the application of land cover in determining roughness coefficients implicitly incorporates both distributive micro roughness (e.g., grass, paddy fields, and surface textures) and macro roughness (e.g., trees and man-made structures). This combined representation enhances the realism of tsunami inundation modeling and provides a more secure assessment of the potential protective role of natural and artificial features surrounding YIA.

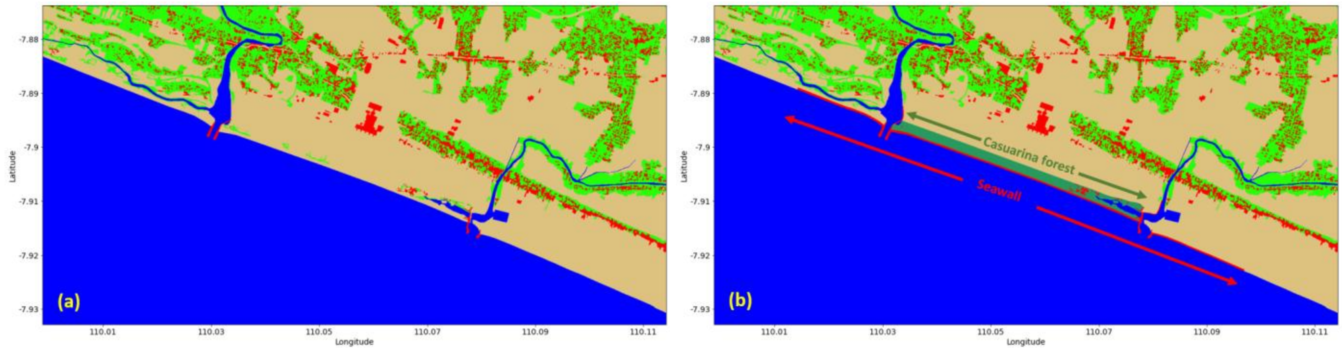

Fig. 5. Land Use/Land Cover (LULC) classification generated from Google satellite imagery. The colors represent different land cover types: blue = water bodies, green = vegetation, tan = open flat areas, and red = man-made buildings. (a) Existing LULC conditions, (b) Modified LULC map showing proposed seawall (red arrow) and *Casuarina* forest (dark green) as coastal protection measures.

Table 3
Surface roughness parameters

Land cover group	Manning's roughness coefficient	Roughness type	Source
Water (e.g., river, pond, sea)	0.025	micro	Harada and Imamura 2006
Open area (e.g., cultivated area, beach, field, road, airport runway)	0.036	micro	Chow 1959
Vegetation (e.g., shrubs, bushes, trees)	0.046	macro	Chow 1959
Casuarina forest	NA / Morison equation	macro	Morison et al. 1950; Harada and Kawata 2004, 2005
Man-made building (e.g., residential, airport building, break water, seawall)	0.060	macro	Wang et al. 2020; Wang et al. 2017

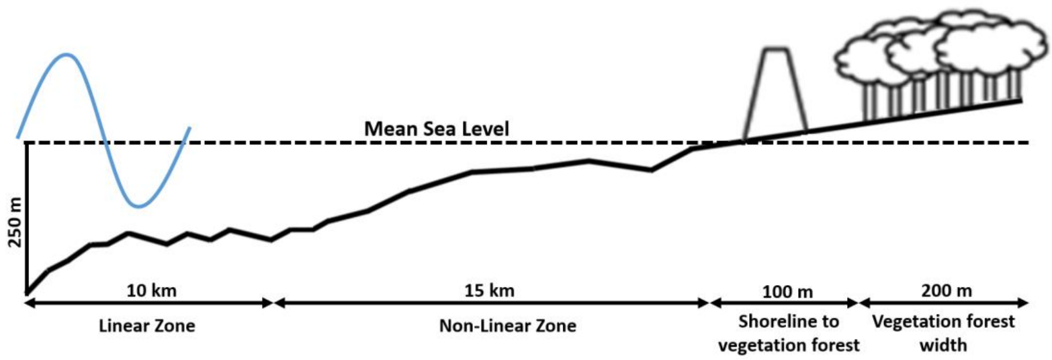

Fig. 6. Cross-sectional schematic of elevation profile from offshore to inland forest vegetation

Fig. 6 shows the land elevation profile. The seawall is positioned 50 meters inland from the shoreline, while the vegetation belt begins 100 meters further inland. A 200-meter-wide *Casuarina equisetifolia* forest was designed near the coastline to help prevent tsunami waves from reaching the airport area. The parameters of the forest were defined as follows: 10 trees per 100 m^2, a trunk diameter of 0.2 meters, a standardized tree height of 12 meters, and a canopy width of 3 meters. This forest belt, extending 5.4 kilometers between the Bogowonto and Serang rivers, was manually delineated using GIS-based software. Within this defined area, the model applied resistance forces to simulate the barrier effect of *Casuarina* trees against incoming tsunami waves. This approach enables realistic simulation of wave-vegetation interactions and their effects on tsunami wave attenuation and inland inundation.

3. Results and discussion

This section presents the results of tsunami inundation modeling for eight different mitigation scenarios. The simulation results show that the tsunami waves began reaching the coastline approximately 32 minutes after the initial earthquake (see **Fig. 13**). Maximum offshore wave heights near the coast ranged from 5 to 9 meters, depending on bathymetric variations. As the waves approached the coastline and entered shallower areas, their height increased due to shoaling effects. The predicted maximum water depth in the study area exceeds 20 meters (see **Table 4**), particularly in areas with elevations below 5 meters. This result is consistent with tsunami modeling by Widiyantoro et al. (2020), Prabowo et al. (2024) and Wulandani et al. (2024), who reported peak tsunami heights of approximately 20 meters for megathrust rupture scenarios along the southern Java. The simulations also showed that most of the airport runway and terminal area would be inundated under these conditions, highlighting the vulnerability of critical infrastructure. The effectiveness of the eight mitigation scenarios is analyzed from spatial, statistical, and temporal perspectives.

3.1. Spatial analysis of inundation areas across mitigation scenarios

Based on the water inundation map presented in **Fig. 7**, the scenario without structural or nature-based protection (scenario 1) results in the worst impact when a major tsunami occurs. Tsunami wave propagation tends to follow natural topographic features such as river channels and basins, which significantly increases the vulnerability of the area surrounding Yogyakarta International Airport. After reaching land, the tsunami rapidly inundates low-lying coastal areas, with water advancing up to 2.5 kilometers inland in some locations. Areas along the coastline experience significant inundation depths, reaching between 8 and 20 meters. The absence of structural defenses and the limited extent of natural vegetation allow deep and extensive wave penetration into the airport zone.

A comparison of the inundation maps for scenario 1 (existing LULC conditions) and scenario 3 (installation of a 5-meter seawall) reveals that the pattern and extent of inundation appear visually very similar. This demonstrates that a 5-meter-high seawall is insufficient to mitigate inundation caused by tidal waves or tsunamis. When incoming waves exceed 5 meters, the water can overtop or even damage the seawall, allowing water to continue inland. Therefore, a 5-meter-high seawall may provide protection only against small to medium-sized waves but is ineffective against larger and stronger waves. Observations from Japan's 2011 tsunami on the Tohoku coast also indicate that several seawalls were overtopped or damaged under extreme wave loads, particularly where the incident wave height exceeded the barrier height (Raby et al. 2015; Fukutani et al. 2023).

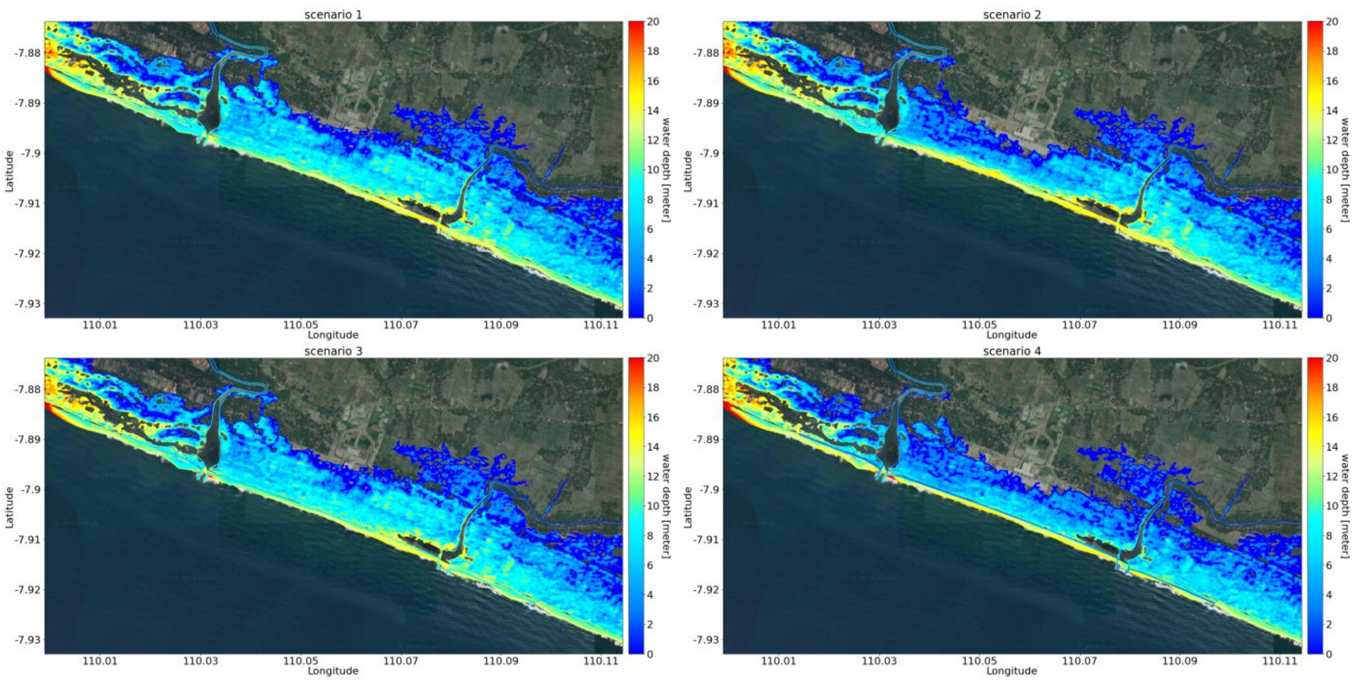

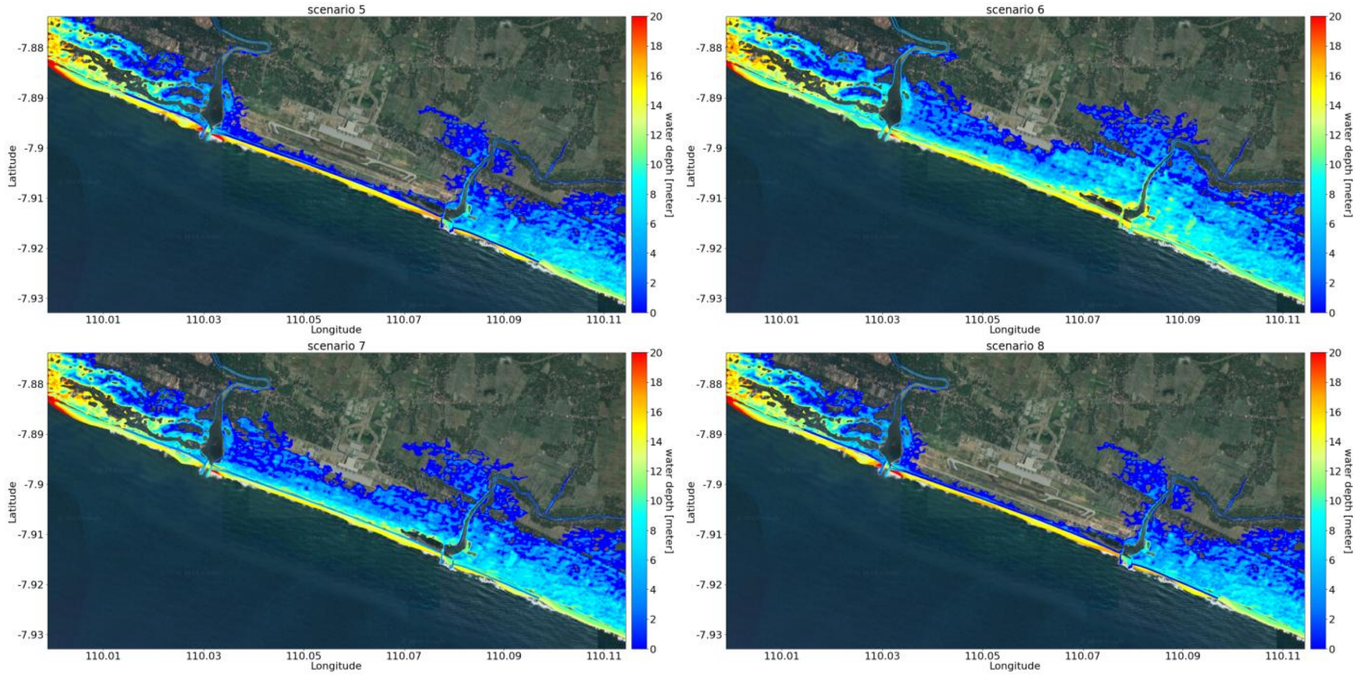

Fig. 7. Maps of maximum inundation depth resulting from a tsunami event for eight scenarios. The color scale on the right indicates the maximum water depth, ranging from light blue (shallow) to red (deep).

When a vegetation-based barrier (scenario 2) is implemented, spatial inundation patterns begin to shift. Areas located behind the vegetative belts experience notable reductions in depth, even though locally. *Casuarina equisetifolia* trees act as wave energy buffers that disperse momentum before it reaches vital infrastructure such as airport buildings. However, they are not sufficiently effective in countering high-energy waves and in certain locations they may even generate turbulence or backflow that increases local inundation depths. This pattern is align with the observations from the 2004 Indian Ocean tsunami, where *Casuarina* and mangrove forests in Sri Lanka, India, and Thailand attenuated wave energy but were unable to fully prevent inundation under extreme conditions (Tanaka et al., 2007; Samarakoon et al., 2013). The consistency between these results suggests that vegetation barriers provide measurable but limited protection, and that their effectiveness depends heavily on forest width, density, and tree morphology (Mukherjee et al., 2023; Chen et al., 2025).

While vegetation offers partial attenuation, the addition of structural measures further modifies inundation dynamics. The results show that this pattern does not change significantly even when a 10-meter-high seawall is implemented (see scenarios 2 and 4 in **Fig. 7**). This indicates that local topographic and hydrological networks play a dominant role in determining the distribution of tsunami inundation. The 15-meter seawall, however, demonstrates a much greater effectiveness in limiting both inland penetration and inundation depth. The inundated area is markedly reduced, and even the airport area remained unaffected by tsunami flooding.

Similar behavior has been documented in experimental studies conducted by Oda et al. (2018), who showed that low seawalls are easily overtopped during large tsunami waves, leading to high inundation depths behind the structure, whereas increasing the wall height substantially reduces inland flooding. Likewise, McGovern et al. (2023) demonstrated through large-scale laboratory experiments that higher seawalls significantly reduce flow penetration and inundation area, although localized overtopping and reflection can still occur depending on site topography. These findings reinforce the current study's results, confirming that higher seawalls are much more effective in mitigating extreme tsunami impacts.

However, unlike purely structural approaches, the integration of vegetation in this study shows that natural elements can further dissipate overtopping energy and improve resilience, a principle supported by hybrid defense research in Europe and Japan (Morris et al. 2023; Zanin et al. 2024). These comparative findings position the YIA mitigation strategy within a broader global discourse on multi-layered coastal protection, demonstrating that combining seawalls with ecological barriers provides both enhanced safety and environmental sustainability.

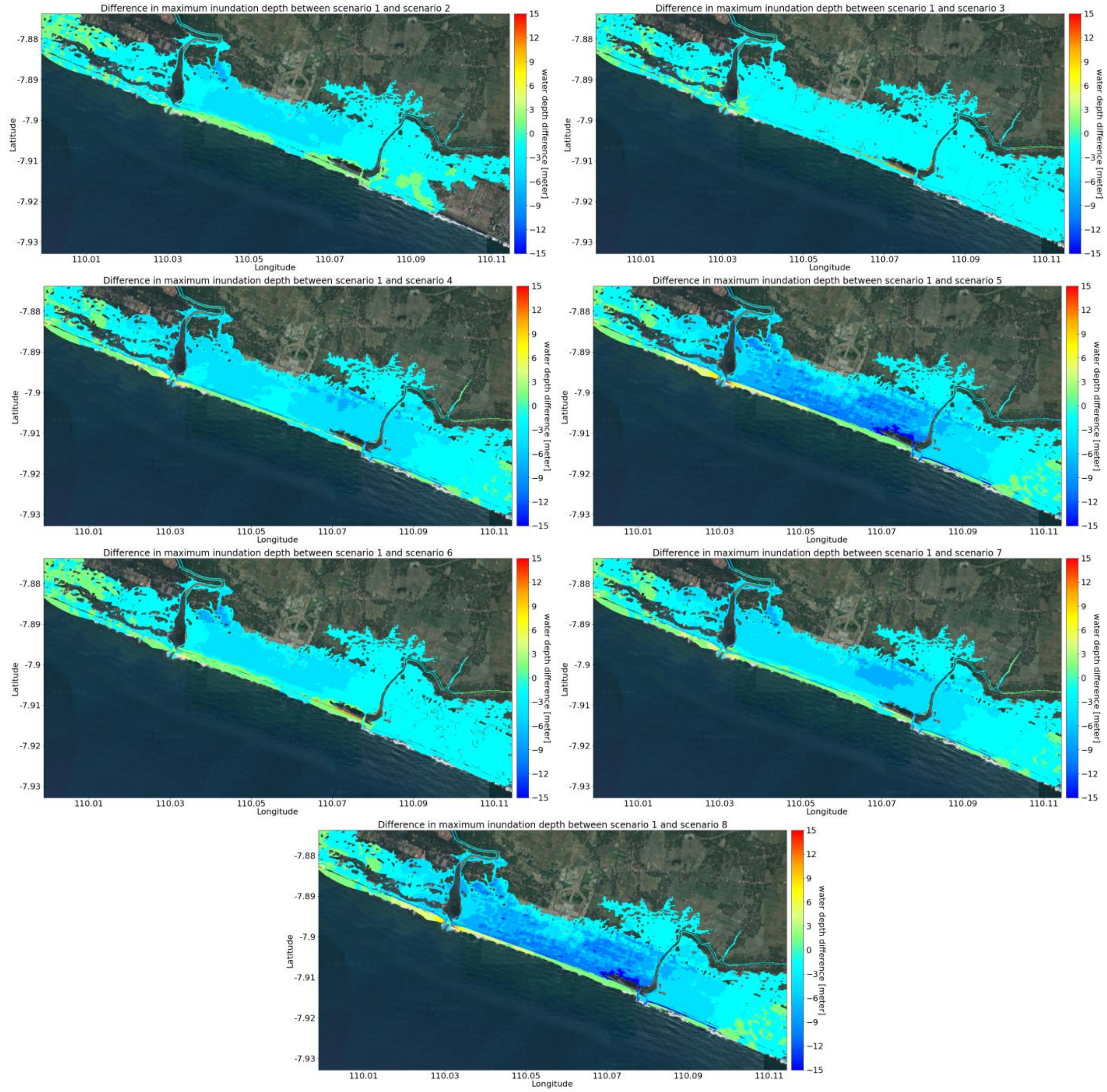

Fig. 8. Difference in maximum inundation depth between a baseline scenario (scenario 1) and other scenarios. The color scale indicates the water depth difference in meters.

Fig. 8 presents a comparative analysis of the effectiveness of various tsunami mitigation scenarios by spatially visualizing the differences in maximum inundation depth between each mitigation scenario and the baseline scenario (scenario 1). The inundation depth difference maps use a color scale where positive values (green to red) indicate increased depth and negative values (light to dark blue) indicate reduced depth. These maps offer qualitative spatial insights into the impact of each mitigation strategy. A comparison between Scenario 1 and Scenario 2 reveals a decrease in inundation depth across most land areas, as reflected by the predominance of light to medium blue colors. This indicates that the presence of *Casuarina equisetifolia* vegetation, although passive, is quite effective in reducing inundation depth. The decrease in depth is most pronounced in areas between the Bogowonto and Serang rivers, where this vegetation can act as a natural barrier. However, there are small patches of yellow or orange near the shoreline or in river channels, indicating the potential for localized increases in depth due to complex interactions between waves and vegetation structure or changes in flow patterns.

The use of a 5-meter seawall did not result in a significant reduction in inundation depth. However, increasing the seawall height to 10 meters (scenario 4) and 15 meters (scenario 5) clearly demonstrated a dramatic increase in effectiveness. Based on the depth difference map between scenario 1 and scenario 4, most of the areas that are inundated by deep flooding in the existing LULC condition are now dominated by dark blue in the mitigation scenario 4, which indicates a significant decrease in inundation depth (up to 6-9 meters). This effect is most pronounced in the area behind the seawall. However, small patches of yellow or orange remain in front of the seawall along unprotected sections of the coastline and around river mouths, indicating localized increases in depth caused by concentrated wave energy. This pattern is consistent with field observations from the 2011 Great East Japan Earthquake and Tsunami by Lipscy et al. (2013), where overtopping and focused energy around river mouths occurred despite the presence of high seawalls. Scenario 5 shows even greater coverage and higher intensity of dark blue, showing a substantial reduction in inundation depth of up to 15 meters across a wider area. This confirms that the 15-meter seawall is the most effective strategy for reducing tsunami inundation depth.

3.2. Statistical analysis across mitigation scenarios

A summary of the total inundation area and the maximum inundation depth (h_{max}) for each scenario is presented in **Table 4**. The parameters P50 (median), P75, and P98 represent the statistical percentiles of the maximum inundation depth, while Max_h_{max} denotes the highest maximum inundation depth in the study area. The statistical results show that mitigation scenarios 2, 3, and 6 do not have significant effects on reducing either the inundation area or water depth. Scenarios involving taller seawalls demonstrated a stronger impact in reducing inundation. A 10-meter seawall (scenario 4) significantly decreases the inundation area to 17.56 km^2 and reduces the median depth to 4.61 m. A 15-meter seawall (scenario 5) is statistically very effective in reducing inundation, reducing the inundation area to 12.10 km^2 and the median depth to 4.44 m. Interestingly, the increase in seawall height is accompanied by a rise in the highest water depth (Max_h_{max}), reaching 30.68 meters in scenario 5. This phenomenon is caused by waves bouncing after hitting a higher seawall, which may cause an increase in local inundation height on the seaward side (Motoyashiki et al. 2024; Parady et al. 2018). Nevertheless, the median and percentile water depths (P50, P75, P98) generally show a downward trend, indicating that although there are some locations with extreme depths, the overall area affected by high water depths is decreasing. The 15-meter seawall, in particular, is highly effective in preventing wave propagation toward critical facilities such as the airport. The combination of CE and a 15-meter seawall (Scenario 8) is the most effective scenario, yielding the smallest inundation area of 11.98 km^2. CE helps dampen the wave energy that overtops the seawall and prevents the overflow force from reaching the airport area. This indicates that the combination of natural and structural measures provides optimal mitigation for retaining and reducing tsunami energy.

Table 4
Summary of inundation parameters for different mitigation scenarios

Scenario	Mitigation scenario	Total area of inundation [km^2]	Max_h_{max} [meter]	Mean_h_{max} [meter]	Statistic_h_{max} Percentile [%]	[meter]
1	Existing LULC	20.45	20.84	6.57	P50	6.43
					P75	9.32
					P98	15.04
2	*Casuarina equisetifolia* (CE)	19.02	21.14	6.33	P50	5.55
					P75	9.23
					P98	15.72
3	5-meter seawall	20.31	22.23	6.50	P50	6.36
					P75	9.14
					P98	15.14
4	10-meter seawall	17.56	28.14	5.65	P50	4.61
					P75	7.71
					P98	15.75
5	15-meter seawall	12.10	30.68	5.90	P50	4.44
					P75	8.77
					P98	16.86
6	5-meter seawall + CE	18.91	22.43	6.28	P50	5.48
					P75	9.20
					P98	15.90
7	10-meter seawall + CE	17.08	27.91	5.63	P50	4.40
					P75	8.04
					P98	15.81
8	15-meter seawall + CE	11.98	30.75	5.95	P50	4.52
					P75	8.85
					P98	16.86

In contrast to the previous approach which examined the total inundation area, **Fig. 9** further explores the distribution of maximum water depth (h_{max}) for each mitigation scenario. The inundation area is segmented by water depth, with each colored segment representing a specific depth range. The numerical values within each segment indicate the area in km^2 for that specific depth range, while the number at the top of each bar represents the total maximum inundation area for that scenario. Areas with moderate to high inundation depths (ranging from 1 to 10 meters) are the most extensively flooded zones. In scenarios 1, 2, 3, 4, 6, and 7, these zones account for more than 70% of the total inundated area, while in scenarios 5 and 8, they comprise approximately 65%. This indicates a potentially high risk of structural damage and loss of life if a major tsunami occurs. In scenarios 5 to 8, areas with the inundation depths below 10 meters decrease significantly. In these scenarios, the YIA area is substantially protected by the presence of the seawall (see **Fig. 7**). The 15-meter-high seawall plays a crucial role in preventing tsunami wave energy from entering the airport area.

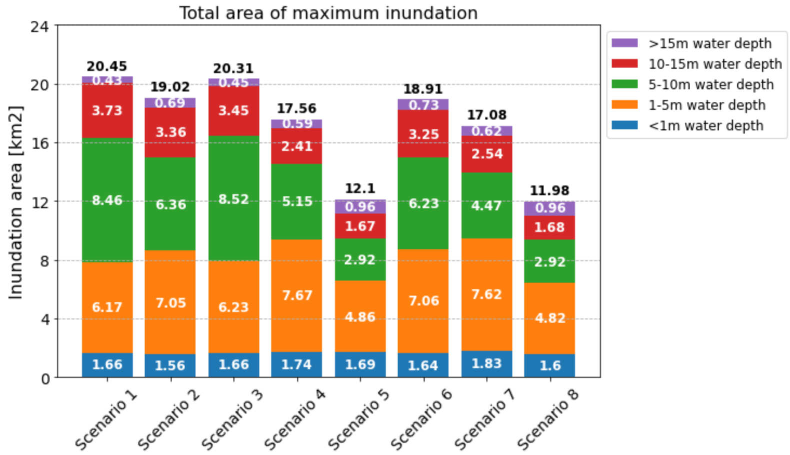

Fig. 9. Total area of maximum inundation at different water depth categories across eight mitigation scenarios

The graph in **Fig. 10** provides a comprehensive overview of how much area is submerged at a given depth, while the scatterplot in **Fig. 11** specifically compares the impact of mitigation at each pixel location. In **Fig. 10**, it is clear that the scenario with the existing LULC (blue line) almost overlaps with the scenario using a 5-meter seawall (red line). This indicates that the addition of a 5-meter seawall does not have a significant impact on the total inundation area (see also **Fig. 7**). However, even though the graph appears to overlap, based on the scatterplot in **Fig. 11**, the use of a 5-meter seawall is quantitatively proven to reduce flood depth over a large area (14.23 km²). Despite these seemingly contradictory data, it can be concluded that inundation depth decreases in certain areas while increasing in others. However, the area experiencing depth reduction is considerably larger than the area experiencing increased depth. A similar pattern is observed in the natural barrier implementation (green line) which overlaps with the "CE + seawall 5m" graph (orange line), indicating that the addition of a 5-meter seawall to *Casuarina equisetifolia* (CE) vegetation does not provide a significant additive effect on the total inundation area.

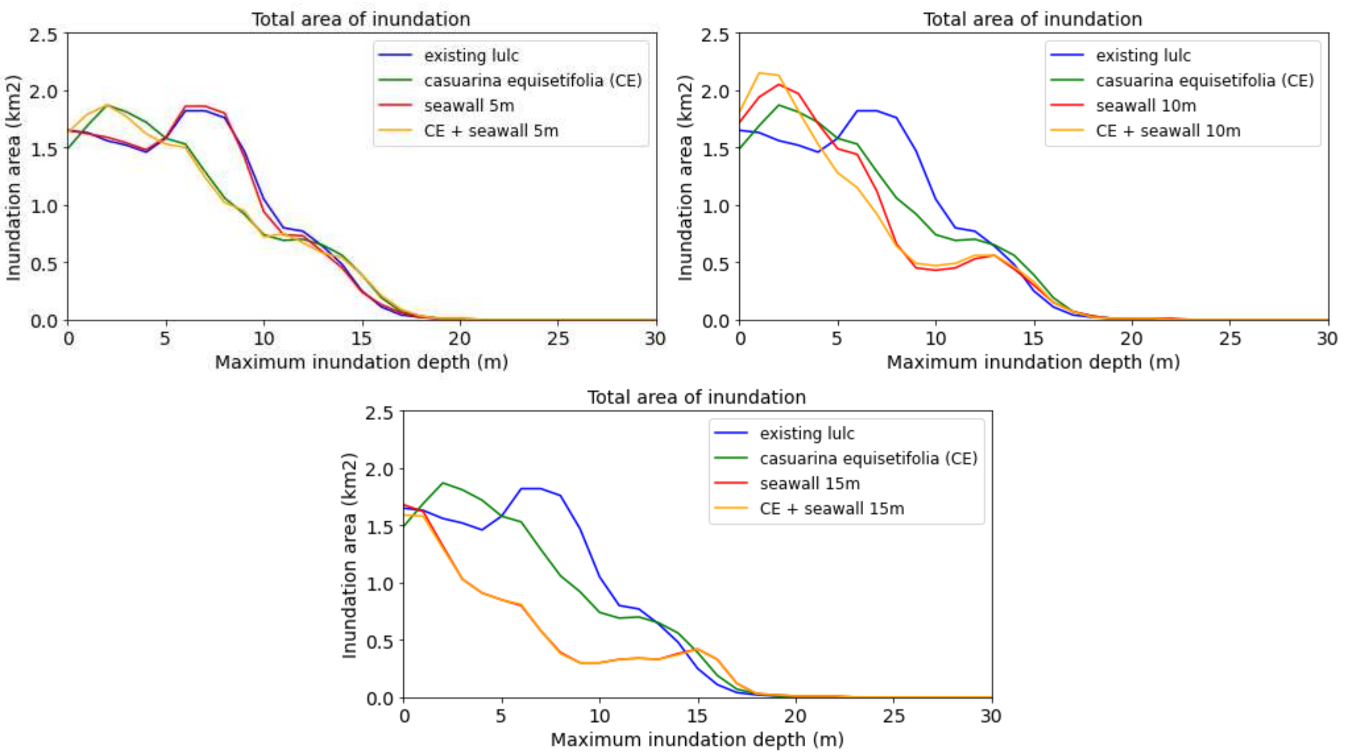

Fig. 10. Histogram of the relationship between total inundation area (km2) and maximum inundation depth (m) for various mitigation scenarios

When the seawall height is increased to 10 meters, more significant changes are observed. The "seawall 10m" graph (red line) and its combination with the CE (orange line) show a substantial reduction in inundation area at depths between 5 and 15 meters compared to the existing condition. The scatterplot clearly shows that mitigation scenarios 4 and 7 resulted in a reduction of inundation area by 16.06 km² and 15.87 km², respectively, compared to the existing LULC scenario. This corresponds to a reduction of nearly 78% of the total inundated area. Furthermore, the effect of mitigation strategy using a 15-meter-high seawall is also clearly visible. The use of the 15-meter seawall alone (red line), or in combination with *Casuarina equisetifolia* (CE) (orange line), significantly reduces the total inundation area. Orange and red curves appear to overlap closely and consistently lie below the other curves, particularly at depths less than 14 meters (see **Fig. 10**). The scatterplot diagram supports this, showing that an area of approximately 16.4 km² experiencing a decrease in depth. This confirms that a 15-meter seawall, either alone or in combination with a CE, is the most effective mitigation solution in reducing the overall inundation depth in the study area.

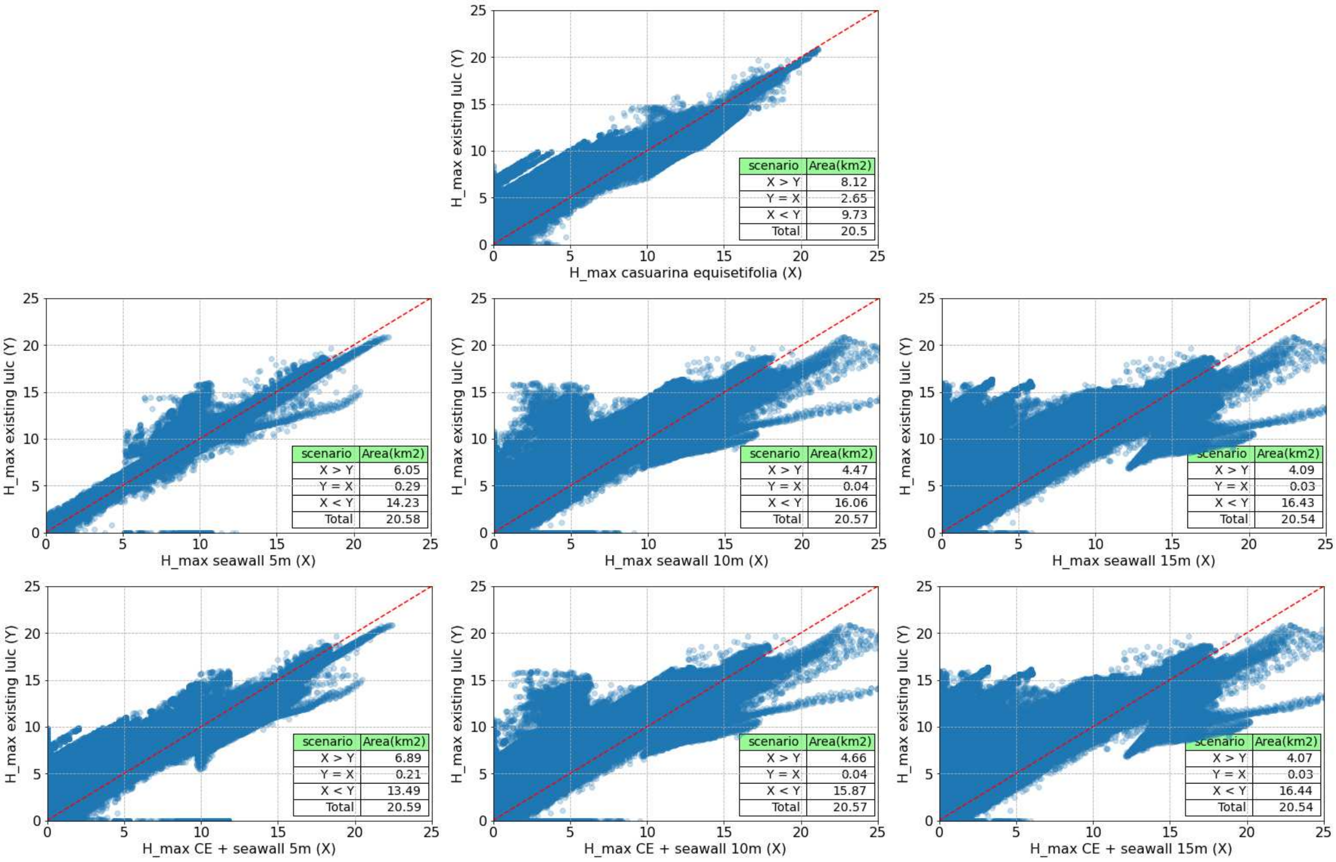

Fig. 11. Scatterplot diagrams comparing the maximum inundation depth (h_{max}) between the existing LULC scenario (Y-axis) and other mitigation scenarios (X-axis). The dashed red line represents the Y=X condition, where inundation depths are equal for both scenarios.

3.3. Temporal analysis of inundation area across mitigation scenarios

Temporal aspects are critical when discussing preparedness and resilience, particularly for infrastructure such as airports that play vital roles in emergency response. Tsunamis may impact the coast by a series of waves, as shown by the simulated time series in **Fig. 12**. Consequently, coastal areas may be inundated multiple times, as indicated by the observation points (P1, P2, and P3) for each scenario in **Fig. 12**. The first tsunami peak reached observation points P2 and P3 approximately 35 minutes after the earthquake, while at P1 it arrived slightly later, around 40 minutes post-event. This is consistent with the numerical modeling by Widiyantoro et al. (2020) and Widodo et al. (2024), which indicated that tsunamis generated by the Java megathrust segments can reach the southern coast of Java within approximately 30–35 minutes, producing near-field wave heights exceeding 20 meters along the shoreline. The airport may be inundated by the first wave, opening more space for subsequent waves to penetrate further inland. Under successive wave impacts, buildings may sustain progressive damage, which continue to alter the flow patterns. The highest water level occurs at point P3, exceeding 15 meters above sea level. This is primarily due to the inflow of water from the southeast, which entered through the Serang River.

Fig. 13 shows the temporal evolution of inundation across depth categories over the 90-minute simulation. The results show that in all scenarios, tsunami waves began to reach the coastline approximately 32 minutes after the megathrust earthquake occurred. During the first 15 minutes after the tsunami waves reached the coastline, depth categories of 1–5 meters became dominant, followed by areas submerged at 5–10 meters, indicating that much of the area, including the airport, faces moderate to deep flooding.

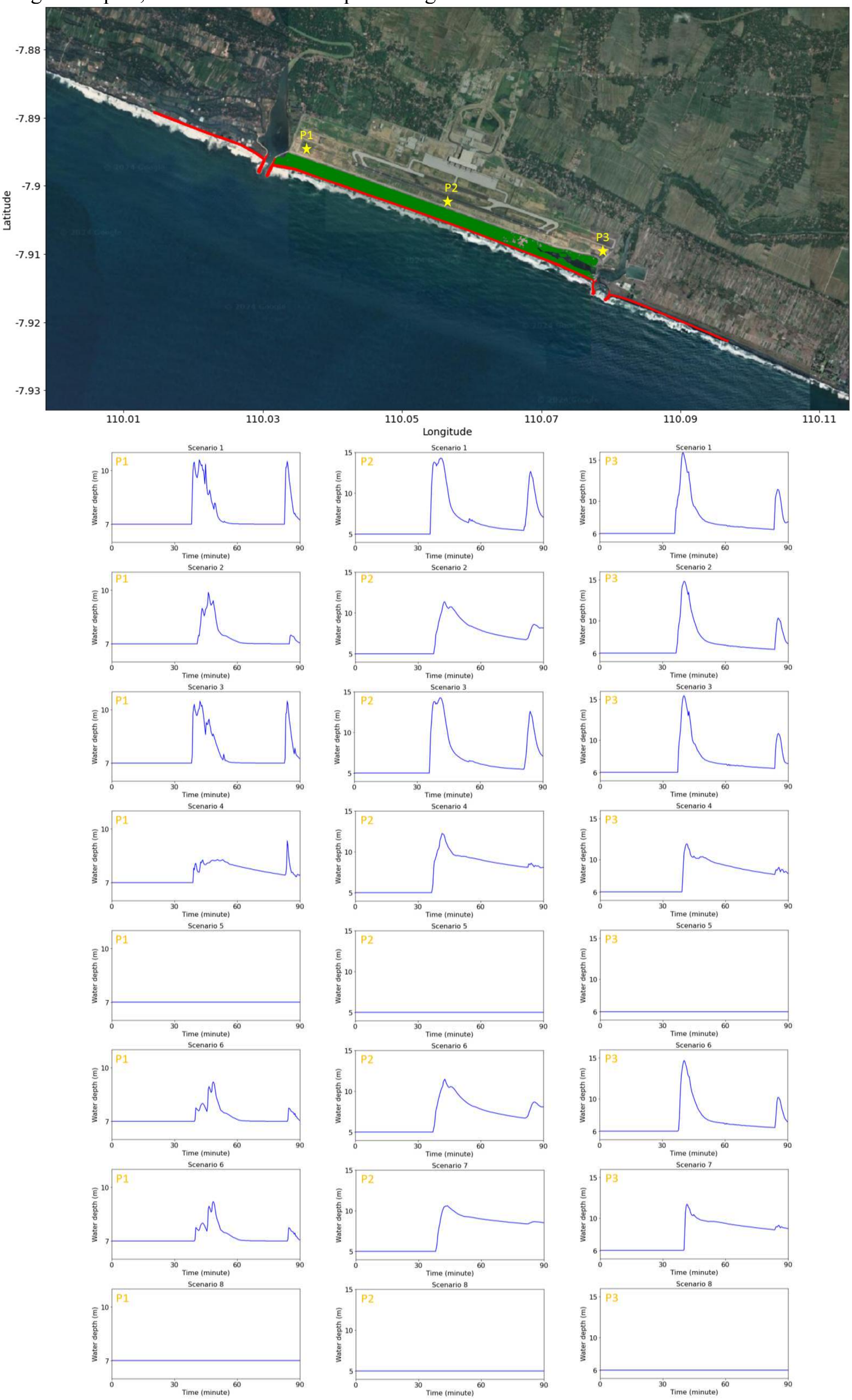

Fig. 12. Simulated time series of tsunami water levels, reference to mean sea level, at three observation points (P1, P2, and P3) under eight different mitigation scenarios

In the scenario using existing condition (scenario 1), CE barrier (scenario 2), and scenarios using a 5-meter seawall (scenario 3 and scenario 6), areas with depth of 1-5 meters (green line) increased rapidly, reaching a peak above 10 km² around the 45th minute. Simultaneously, areas with depth of 5-10 meters (red line) also showed a significant rise, reaching nearly 8 km². Although the area inundated by depths greater than 10 meters (orange line) was relatively small, it still showed a momentary peak exceeding 1 km², indicating the presence of highly hazardous zones, particularly near coastal and riverine lowlands. Over time, the water began to spread and infiltrate, causing the shallower depth area (<1 meter, blue line) to gradually increase, reaching a peak above 8 km² around the 60th minute. Then, after about the 70th minute, a receding trend was observed, with the deeper depth area beginning to decrease. However, a secondary peak in the 5-10 meter and >10 meter depth areas occurred at the 80th minute. This phenomenon may suggest the occurrence of a secondary wave or indicate the complex hydrodynamic behavior of wave backflow during the later stages of inundation.

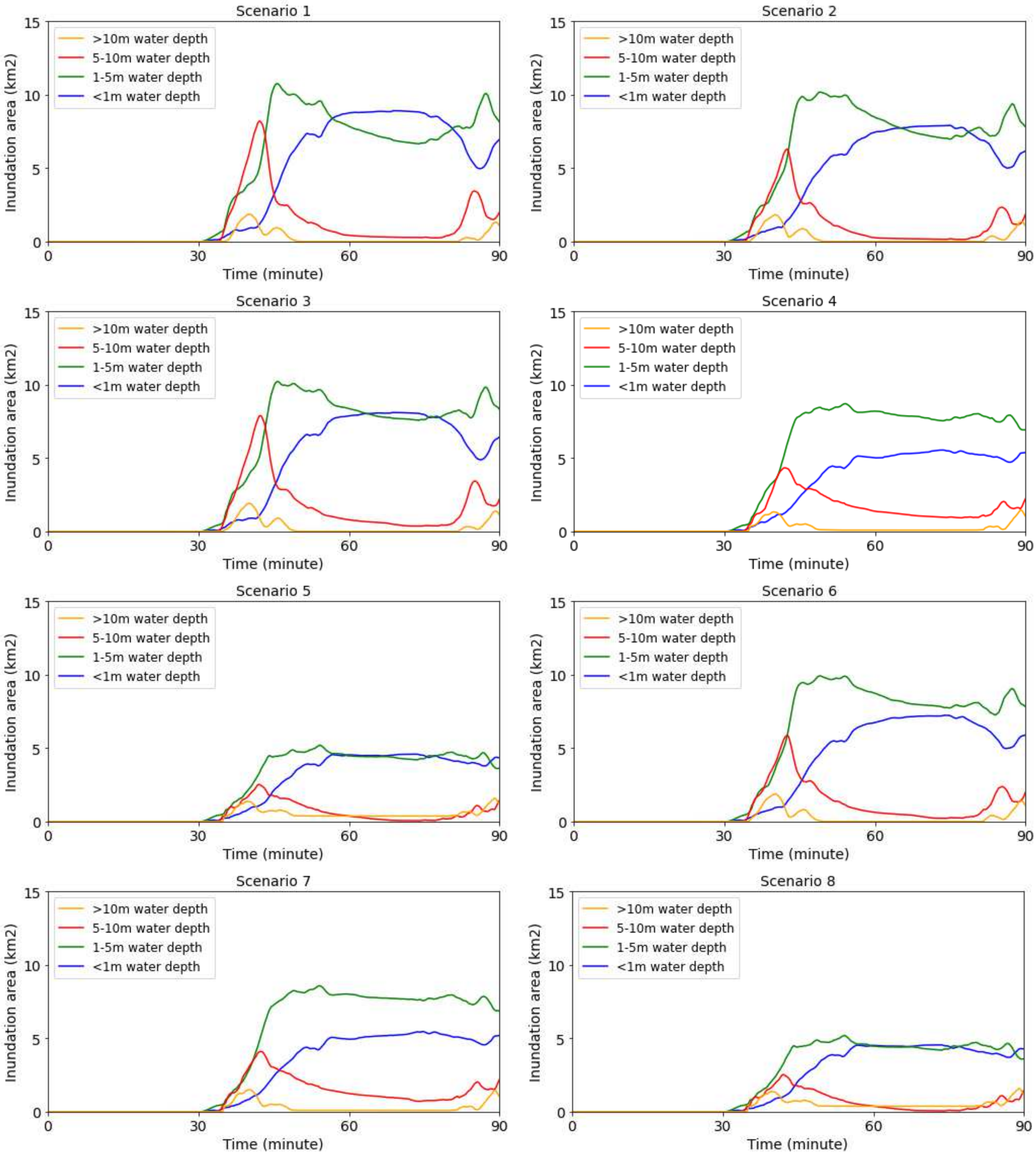

Fig. 13. The temporal evolution of total inundation area for different water depth categories over a 90-minute simulation period

The CE vegetation scenario (scenario 2) does little to alter this temporal pattern. While it slightly delays wave penetration, its effects are limited in reducing inundation speed or duration. This suggests that CE plays a more relevant role during the initial wave arrival phase as a first line of defense but is insufficient to significantly transform the overall inundation dynamics. Significant changes occur with the implementation of 15-meter seawall. This scenario shows a marked temporal shift, high-depth areas emerge later and in reduced extents. In other words, a high seawall not only physically blocks tsunami waves but also delays the peak flooding time, thereby providing additional time for evacuation or the implementation of emergency measures to protect vital facilities (Parady et al. 2018; Esteban et al. 2017). In simulations, hybrid scenarios with CE and tall seawalls produce similar temporal effectiveness to seawalls alone, emphasizing that substantial changes in flood timing are driven more by structural barriers than vegetation.

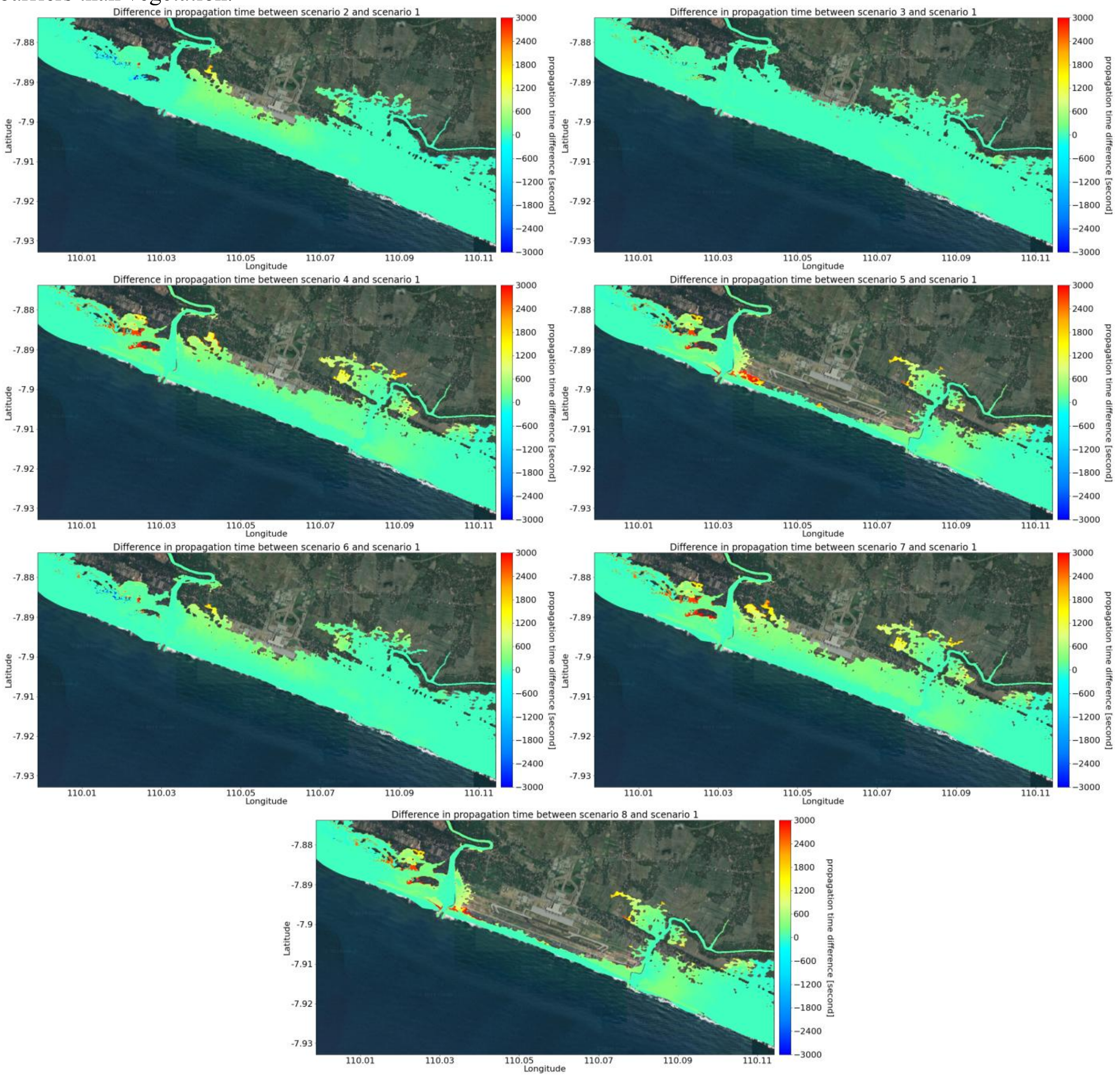

Fig. 14. Difference in tsunami wave propagation time between baseline scenario (scenario 1) and other scenarios in seconds. Positive values (green to red) indicate a delay in wave arrival time compared to the baseline (scenario 1), while negative values (light to dark blue) indicate earlier wave arrival.

As shown in **Fig. 14**, the scenario with a *Casuarina* forest belt (Scenario 2) provides moderate protection, although the effect is spatially limited, with propagation delays of approximately five minutes occurring primarily near vegetated areas. Scenario 3 (5-meter seawall) shows no change in arrival times, indicating that a low seawall is insufficient to significantly alter tsunami propagation. In contrast, scenarios involving higher seawalls (10 meters and 15 meters) demonstrate more pronounced effects, with wider zones of delayed wave propagation, particularly in low-lying coastal areas. The scenario using a 15-meter seawall shows the greatest propagation delays, especially near river mouths and coastal settlements. Vegetation alone is moderately effective, whereas seawalls higher than 10 m substantially improve coastal resilience. The combined scenarios (7 and 8), which integrate vegetation and high seawalls, emerge as the most effective approach, providing synergistic benefits by reducing wave energy offshore and limiting inland penetration. These findings highlight the importance of hybrid coastal defense strategies in maximizing tsunami risk mitigation.

4. Conclusions

This study provides new insights into the effectiveness of multi-layered coastal defense systems for mitigating tsunami inundation risks in subduction zone environments. Using high-resolution numerical simulations under a worst-case Mw 8.8 megathrust earthquake scenario, the analysis demonstrates that the combination of structural and nature-based measures can substantially enhance coastal resilience. Among the tested configurations, seawalls higher than 10 meters markedly reduce inundation depth and extent, while a 15-meter seawall nearly eliminates flooding within the modeled coastal infrastructure zone. These structural defenses also delay tsunami arrival times, providing critical additional minutes for evacuation and emergency response an important aspect often overlooked in single-layer mitigation strategies.

Nature-based solutions, represented by *Casuarina equisetifolia* forests, also exhibited important protective benefits. Although the vegetation belt alone was insufficient to counter extreme wave energy, its role became increasingly valuable when combined with seawalls. The hybrid scenarios, particularly the integration of a 15-meter seawall with a 200-meter-wide Casuarina belt, achieved the greatest overall effectiveness by dissipating overtopping energy and reducing residual flooding. Such integrated strategies are consistent with global best practices that emphasize the combination of engineered and ecological defenses to maximize coastal safety while also preserving ecosystem services.

Beyond the specific case context, the findings contribute to a broader understanding of tsunami risk mitigation in low-lying, high-exposure regions worldwide. Airports, ports, and power plants located near vulnerable shorelines require robust defense systems that are not solely reliant on single structures. Instead, a multi-layered approach that blends physical barriers with ecological buffers offers the most effective approach to reducing tsunami risk and ensuring operational resilience during extreme events.

There remains considerable room for advancement in this area of research. Future work should investigate the optimal placement of different protective structures and assess the most effective shape of the seawall under various tsunami conditions. In addition, large-scale physical modeling experiments are needed to further validate and improve the numerical predictions, thereby strengthening the design basis for integrated coastal defense strategies.

Authors contribution:

Conceptualization: Yudhi Prabowo, Widjo Kongko; Methodology and Software: Yudhi Prabowo, Widjo Kongko; Formal analysis: Yudhi Prabowo, Mardi Wibowo; Visualization: Yudhi Prabowo; Writing – original draft: Yudhi Prabowo; Writing – review and editing: Yudhi Prabowo, Widjo Kongko, Mardi Wibowo, Imam Fachrudun, Fajar Yulianto, Edwin Adi Wiguna, Marindah Yulia Iswari; Data Curation: Yudhi Prabowo, Hanah Khoirunnisa, Hilmi Aziz, Nurkhalis Rahili; Resource: Widjo Kongko, Hanah Khoirunnisa; Supervision: Widjo Kongko. The main contributors are Yudhi Prabowo, Widjo Kongko, and Mardi Wibowo.

Funding

This study was supported by the internal research program of the Research Center for Hydrodynamics Technology, National Research and Innovation Agency (BRIN), Indonesia in 2025.

Data availability

The database are available upon request. Interested readers should make a request to the corresponding author.

Acknowledgments

This research was conducted as part of the ongoing activities of the Coastal Morphodynamics Research Group at the Research Center for Hydrodynamics Technology, National Research and Innovation Agency (BRIN), Indonesia. We extend our sincere appreciation to our colleagues at BRIN for their insightful discussions and valuable suggestions throughout this project. We deeply appreciate the anonymous reviewers for their constructive feedback and thoughtful comments, which significantly contributed to the improvement of this manuscript.

Declaration

Conflict of interests:

The authors declare that they have no conflict of interest.

References

Badan Informasi Geospasial (BIG) (2024) Demnas. https://www.big.go.id/en/content/produk/demnas. Accessed 25 Januari 2025
Bernard E, Titov V (2015) Evolution of tsunami warning systems and products. Philos Trans R Soc A Math Phys Eng Sci 373:20140371. https://doi.org/10.1098/rsta.2014.0371
Boulenger A, Lanza-Arroyo P, Langedock K, Semeraro A, Van Hoey G (2024) Nature-based solutions for coastal protection in sheltered and exposed coastal waters: integrated monitoring program for baseline ecological structure and functioning assessment. Environ Monit Assess 196:316. https://doi.org/10.1007/s10661-024-12480-x
Bricker JD, Gibson S, Takagi H, Imamura F (2015) On the Need for Larger Manning's Roughness Coefficients in Depth-Integrated Tsunami Inundation Models. Coast Eng J 57(2): 1550005-1 - 1550005-13. https://doi.org/10.1142/S0578563415500059
Cheng W, Weiss R (2013) On sediment extent and runup of tsunami waves. Earth Planet Sci Lett 362:305-309. https://doi.org/10.1016/j.epsl.2012.12.004
Chen Y, Cao Z, Chen Y, Wang L, Shan L, Yu S, Yang W, Liu J, Yu K (2025) Evaluation of the stand quality of Casuarina equisetifolia in coastal shelterbelts. J Mt Sci 22:1557-1570. https://doi.org/10.1007/s11629-024-9265-9
Chow VT (1959) Open-channel hydraulics. McGraw-Hill Book Co., New York
Dewatama E, Ikaputra (2021) Tsunami hazard mapping and loss estimation in Yogyakarta International Airport area. Built Environ Stud 2:1–11. https://doi.org/10.22146/best.v2i1.535
de Ruig JHM (1998) Seaward coastal defence: limitations and possibilities. J Coast Conserv 4:71–78. https://doi.org/10.1007/BF02806492
Dogan GG, Annunziato A, Hidayat R (2021) Numerical simulations of December 22, 2018 Anak Krakatau tsunami and examination of possible submarine landslide scenarios. Pure appl Geophys 178:1–20. https://doi.org/10.1007/s00024-020-02641-7
Esteban M, Glasbergen T, Takabatake T, Hofland B, Nishizaki S, Nishida Y, Stolle J, Nistor I, Bricker J, Takagi H, Shibayama T (2017) Overtopping of coastal structures by tsunami waves. Geosciences 7(4):121. https://doi.org/10.3390/geosciences7040121
Fathianpour A, Evans B, Jelodar MB, Wilkinson S (2024) Environmental factors in tsunami evacuation simulation: topographic, traffic jam, human behaviour. Nat Hazards 120:12797–12815. https://doi.org/10.1007/s11069-024-06714-x
Fukutani Y, Yasuda T, Yamanaka R (2023) Efficient probabilistic prediction of tsunami inundation considering random tsunami sources and the failure probability of seawalls. Stoch Environ Res Risk Assess 37:2053–2068. https://doi.org/10.1007/s00477-023-02379-3
Geist E, Yoshioka S (1996) Source parameters controlling the generation and propagation of potential local tsunamis along the Cascadia margin. Nat Hazards 13:151–177. https://doi.org/10.1007/BF00138481
Griffin J, Nguyen N, Cummins P, Cipta A (2019) Historical earthquakes of the eastern Sunda Arc: Source mechanisms and intensity-based testing of Indonesia's national seismic hazard assessment. Bull Seismol Soc Am 109:43–65. https://doi.org/10.1785/0120180085
Haghdoost M, Azamathulla HM (2024) Predicting the drag coefficient of coastal trees using SVM and boosting ensemble models. Discov Water 4:102. https://doi.org/10.1007/s43832-024-00162-1
Harada K, Imamura F (2000) Experimental study on the resistance by mangrove under the unsteady flow. Proc 1st Congr Asian Pacific Coast Eng, pp 975–984.
Harada K, Imamura F (2006) Effects of coastal forest on tsunami hazard mitigation – a preliminary investigation. In: Tsunamis: Case Studies and Recent Development 23:279–292. https://doi.org/10.1007/1-4020-3331-1_17
Harada K, Kawata Y (2004) Study on the effect of coastal forest to tsunami reduction. Annu Disas Prev Res Inst Kyoto Univ 47C.
Harada K, Kawata Y (2005) Study on tsunami reduction effect of coastal forest due to forest growth. Annu Disas Prev Res Inst Kyoto Univ 48C.
Harig S, Chaeroni, Pranowo WS, Behrens J (2008) Tsunami simulations on several scales — comparison of approaches with unstructured meshes and nested grids. Ocean Dyn 58:429–440. https://doi.org/10.1007/s10236-008-0162-5
Harris R, Meservy W, Sulaeman H, Bunds M, Andreini J, Sharp B, Berrett B, Whitehead J, Carver G, Setiadi G, Hapsoro S, Prasetyadi C (2024) Discovery of imbricated beachrock deposits adjacent to the Java trench, Indonesia: influence of tsunami and storm waves, and implications for megathrust earthquakes. Nat Hazards 120:8209–8238. https://doi.org/10.1007/s11069-023-06327-w
Heidarzadeh M, Mulia IE (2022) A new dual earthquake and submarine landslide source model for the 28 September 2018 Palu (Sulawesi), Indonesia tsunami. Coast Eng J 65:97–109. https://doi.org/10.1080/21664250.2022.2122293

Heidarzadeh M, Pirooz MD, Zaker NH (2009) Modeling the near-field effects of the worst-case tsunami in the Makran subduction zone. Ocean Eng 36:368–376. https://doi.org/10.1016/j.oceaneng.2009.01.004

Imamura F, Yalciner AC, Ozyurt G (1995) Tsunami modelling manual (TUNAMI model). International Research Institute of Disaster Science, Tohoku University. https://www.tsunami.irides.tohoku.ac.jp/media/files/_u/project/manual-ver-3_1.pdf. Accessed 2 January 2025

Irsyam M, Widiyantoro S, Natawidjaja DH, Meilano I, et al. (Eds.) (2017) National team for updating of Indonesia earthquake hazard map, Earthquake source and hazard map of Indonesia 2017. National Center for Earthquake Studies of Indonesia (PUSGEN), Research and Development Agency of Ministry of Public Works and Housing, Indonesia.

Kaiser G, Scheele L, Kortenhaus A, Lovholt F, Romer H, Leschka S (2011) The influence of land cover roughness on the results of high resolution tsunami inundation modeling. Nat Hazards Earth Syst Sci 11:2521–2540. https://doi.org/10.5194/nhess-11-2521-2011

Kakinuma T, Kosugi J (2025) Numerical study on the excitation and propagation of surface/internal waves due to air pressure waves over topography. Water Waves 7:315–348. https://doi.org/10.1007/s42286-024-00099-x

Kongko W, Hidayat R (2014) Earthquake-tsunami in South Jogjakarta Indonesia: potential, simulation models, and related mitigation efforts. IOSR J Appl Geol Geophys 2:18–22. https://doi.org/10.9790/0990-0231822

Lauterjung J, Koltermann P, Wolf U, Sopaheluwakan J (2010) The UNESCO-IOC framework – establishing an international early warning infrastructure in the Indian Ocean region. Nat Hazards Earth Syst Sci 10:2623–2629. https://doi.org/10.5194/nhess-10-2623-2010

Lavigne F, Gomez C, Giffo M, Wassmer P, Hoebreck C, Mardiatno D, Prioyono J, Paris R (2007) Field observations of the 17 July 2006 tsunami in Java. Nat Hazards Earth Syst Sci 7:177–183. https://doi.org/10.5194/nhess-7-177-2007

Lawrence S, Nandasena NAK (2019) Hybrid approach for tsunami protection: effect of embankment-type seawall and vegetation on tsunami reduction. KSCE J Civ Eng 23:2391–2396. https://doi.org/10.1007/s12205-019-1759-6

Lay T, Kanamori H, Ammon CJ, Koper KD, Hutko AR, Ye L, Yue H, Rushing TM (2012) Depth-varying rupture properties of subduction zone megathrust faults. J Geophys Res 117(B4). https://doi.org/10.1029/2011JB009133

Lipscy PY, Kushida KE, Incerti T (2013) The Fukushima Disaster and Japan's Nuclear Plant Vulnerability in Comparative Perspective. Environ Sci Technol 47(12):6082–6088. https://doi.org/10.1021/es4004813

Luschen E, Muller C, Kopp H, Engels M, Lutz R, Planert L, Shulgin A, Djajadihardja YS (2011) Structure, evolution and tectonic activity of the eastern Sunda forearc, Indonesia, from marine seismic investigations. Tectonophysics 508:6–21. https://doi.org/10.1016/j.tecto.2010.06.008

Martínez ML, Kolega J (eds) (2013) Coastal dune restoration: trends and perspectives — chapter: ecosystem services of coastal dune systems for hazard mitigation. Springer. https://doi.org/10.1007/978-3-642-33445-0_20

McGovern DJ, Allsop W, Rossetto T, Chandler I (2023) Large-scale experiments on tsunami inundation and overtopping forces at vertical sea walls. Coast Eng 179:104222. https://doi.org/10.1016/j.coastaleng.2022.104222

Morison JR, O'Brien MP, Johnson JW, Schaaf SA (1950) The force exerted by surface waves on piles. Petrol Trans AIME 189:149–154. https://doi.org/10.2118/950149-G

Morris RL, Fest B, Stokes D, Jenkins C, Swearer SE (2023) The coastal protection and blue carbon benefits of hybrid mangrove living shorelines. J Environ Manage 331:117310. https://doi.org/10.1016/j.jenvman.2023.117310

Motoyashiki R, Nakaza E, Miyazato N, Fukumori M, Tanaka S, Schaab C (2024) The wave run-up and reflection effects of wave breaking and currents on step-type seawalls with high steps. J JSCE 12(1):Article ID 23-00242. https://doi.org/10.2208/journalofjsce.23-00242

Muhari A, Heidarzadeh M, Susmoro H, Nugroho S, Wijanarto AB, Triyono R, Supartoyo, Imamura F (2019) The December 2018 Anak Krakatau volcano tsunami as inferred from post-tsunami field surveys and spectral analysis. Pure appl Geophys 176:5219–5233. https://doi.org/10.1007/s00024-019-02358-2

Mukherjee A, Cajas JC, Houzeaux G, Lehmkuhl O, Suckale J, Marras S (2023) Forest density is more effective than tree rigidity at reducing the onshore energy flux of tsunamis: evidence from LES with fluid–structure interactions. Coast Eng 182:104286. https://doi.org/10.1016/j.coastaleng.2023.104286

Ndiaye P, Mailly D, Pineau M, Margolis HA (1993) Growth and yield of Casuarina equisetifolia plantations on the coastal sand dunes of Senegal as a function of microtopographic. For Ecol Manage 56:13–28. https://doi.org/10.1016/0378-1127(93)90100-2

Oda Y, Honda T, Omata T (2018) Experimental study on tsunami forces acting on vertical seawalls under overflow. Coast Eng Proc 1(36):37. https://doi.org/10.9753/icce.v36.papers.37

Okada Y (1985) Surface deformation due to shear and tensile faults in a half-space. Bull Seismol Soc Am 75:1135–1154. https://doi.org/10.1785/BSSA0750041135

Parady G, Tran B, Gilmour S (2018) Effect of seawalls on tsunami evacuation departure in the 2011 Great East Japan Earthquake. Inj. Prev. 25:535–539. https://doi.org/10.1136/injuryprev-2018-042954

Prabowo Y, Kongko W, Wibowo M, Fachrudin I, Yulianto F, Khoirunnisa H, Wiguna EA, Aziz H, Iswari MY, Rahili N (2024) Numerical simulation of seawall and mangrove effectiveness as tsunami barriers for Yogyakarta International Airport. In: 2024 IEEE Asia-Pacific Conference on Geoscience, Electronics and Remote Sensing Technology (AGERS), Indonesia, pp 228–233. https://doi.org/10.1109/AGERS65212.2024.10932941

Rabinovich AB, Thomson RE, Stephenson FE (2006) The Sumatra tsunami of 26 December 2004 as observed in the North Pacific and North Atlantic oceans. Surv Geophys 27:647–677. https://doi.org/10.1007/s10712-006-9000-9

Raby A, Macabuag J, Pomonis A, Wilkinson S, Rossetto T (2015) Implications of the 2011 Great East Japan Tsunami on sea defence design. Int J Disaster Risk Reduct 14:332–346. https://doi.org/10.1016/j.ijdrr.2015.08.009

Samarakoon MB, Tanaka N, Iimura K (2013) Improvement of effectiveness of existing Casuarina equisetifolia forests in mitigating tsunami damage. J Environ Manage 116:372–380. https://doi.org/10.1016/j.jenvman.2012.10.050

Satake K, Ishibe T, Murotani S, Mulia IE, Gusman AR (2022) Effects of uncertainty in fault parameters on deterministic tsunami hazard assessment: examples for active faults along the eastern margin of the Sea of Japan. Earth Planets Space 74:36. https://doi.org/10.1186/s40623-022-01594-6

Setyonegoro W, Hanif M, Khoiridah S, Ramdhan M, Fauzi F, Karima S, Isnaniawardhani V, Pribadi S, Muqqodas MM, Supendi P, Ardhyastuti S (2024) Exploring tsunami generation and propagation: a case study of the 2018 Palu earthquake and tsunami. Kuwait J Sci 51(3):100245. https://doi.org/10.1016/j.kjs.2024.100245

Synolakis C, Imamura F, Tsuji Y, Matsutomi H, Tinti S, Cook B, Chandra YP, Usman M (1995) Damage, conditions of East Java Tsunami of 1994 analyzed. Eos 76(26):257. https://doi.org/10.1029/95EO00150

Tanaka N, Sasaki Y, Mowjood MIM, Jinadasa KBSN, Homchuen S (2007) Coastal vegetation structures and their functions in tsunami protection: experience of the recent Indian Ocean tsunami. Landscape Ecol Eng 3:33–45. https://doi.org/10.1007/s11355-006-0013-9

Tandel P, Patel H, Patel T (2022) Tsunami wave propagation model: A fractional approach. J Ocean Eng Sci 7:509–520. https://doi.org/10.1016/j.joes.2021.10.004

van Veelen TJ, Karunarathna H, Reeve DE (2021) Modelling wave attenuation by quasi-flexible coastal vegetation. Coast Eng 165:103820. https://doi.org/10.1016/j.coastaleng.2020.103820

Varsoliwala A, Singh TR (2021) Mathematical modeling of tsunami wave propagation at mid-ocean and its amplification and run-up on shore. J Ocean Eng Sci 6(4): 367-375. https://doi.org/10.1016/j.joes.2021.03.003

Wang X, Lukovic B, Power WL, Mueller C (2017) High-resolution inundation modelling with explicit buildings: a case study of Wellington CBD. GNS Sci Rep 2017/13:1–27. https://doi.org/10.21420/G2RW2N

Wang X, Power WL, Lukovic B, Mueller C, Liu Y (2020) A pilot study on effectiveness of flow depth as sole intensity measure of tsunami damage potential. Proc N Z Soc Earthq Eng Annu Tech Conf:1–8. https://doi.org/10.5454/NZSEE2020.001

Wells DL, Coppersmith KJ (1994) New empirical relationships among magnitude, rupture length, rupture width, rupture area, and surface displacement. Bull Seismol Soc Am 84:974–1002. https://doi.org/10.1785/BSSA0840040974

Widiyantoro S, Gunawan E, Muhari A, Rawlinson N, Mori J, Hanifa NR, Susilo S, Supendi P, Shiddiqi HA, Nugraha AD, Putra HE (2020) Implications for megathrust earthquakes and tsunamis from seismic gaps south of Java, Indonesia. Sci Rep 10:15274. https://doi.org/10.1038/s41598-020-72142-z

Widodo A B, Nurcahyo A, Hermawan D (2024) Preliminary study of tsunami simulations on megathrust earthquake scenarios in Pacitan Regency, East Java. IOP Conf Ser Earth Environ Sci 1307:012004. https://doi.org/10.1088/1755-1315/1307/1/012004

Wulandani NA, Wibowo YA, Nurwijayanti A (2024) Identification of coastal typology and utilization of geospatial technology for tsunami hazard modeling in Kulon Progo coastal area, Special Region of Yogyakarta, Indonesia. IOP Conf Ser Earth Environ Sci 1357(1):012040. https://doi.org/10.1088/1755-1315/1357/1/012040

Wuthrich D, Pfister M, Schleiss AJ (2019) Effect of bed roughness on tsunami-like waves and induced loads on buildings. Coast Eng 152:1–10. https://doi.org/10.1016/j.coastaleng.2019.103508

Xie F, Wang Z, Zhao D, Gao R, Chen X (2023) Seismic imaging of the Java subduction zone: New insight into arc volcanism and seismogenesis. Tectonophysics 854:229810. https://doi.org/10.1016/j.tecto.2023.229810

Yamaguchi N, Sekiguchi T (2015) Effects of tsunami magnitude and terrestrial topography on sedimentary processes and distribution of tsunami deposits in flume experiments. Sediment Geol 328:115–121. https://doi.org/10.1016/j.sedgeo.2015.08.008

Yoshii T, Tanaka S, Matsuyama M (2017) Tsunami deposits in a super-large wave flume. Mar Geol 391:98–107. https://doi.org/10.1016/j.margeo.2017.07.020

Yoshii T, Tanaka S, Matsuyama M (2018) Tsunami inundation, sediment transport, and deposition process of tsunami deposits on coastal lowland inferred from the Tsunami Sand Transport Laboratory Experiment (TSTLE). Mar Geol 400:107–118. https://doi.org/10.1016/j.margeo.2018.03.007

Zanin GM, Muwafu SP, Costa MM (2024) Nature-based solutions for coastal risk management in the Mediterranean basin: A literature review. J Environ Manage 356:120667. https://doi.org/10.1016/j.jenvman.2024.120667

Zhao S, Cummins PR, McClusky S, Miller MS (2025) Interseismic coupling along the Java–Timor subduction-collision zone in East Indonesia. Geophys Res Lett 52(6). https://doi.org/10.1029/2024GL112563